Hindawi
Advances in Civil Engineering
Volume 2021, Article ID 5564653, 12 pages
https://doi.org/10.1155/2021/5564653

Research Article

Behavior of Hybrid CFRP Laminated Thin-Walled Beams: Experimental, Numerical, and Analytical Evaluations

A. M. Yosri,[1] **Gouda M. Ghanem**,[2] **Mohamed A. E. Salama**,[2] **Majed Alzara**,[1] **Mohamed A. Farouk**,[3] **MD Alhaz Uddin**,[1] **Mohamed AbdelMongy**,[1] **and A. Ehab**[4]

[1]*Department of Civil Engineering, College of Engineering, Jouf University, Sakakah, Saudi Arabia*
[2]*Civil Engineering Department, Helwan University, Mataria Branch, Helwan, Egypt*
[3]*Civil Engineering Department, Delta University, Talkha, Egypt*
[4]*Civil Engineering Department, Badr University, Badr City, Egypt*

Correspondence should be addressed to A. M. Yosri; ahmedyosri198820@gmail.com and Majed Alzara; majedzara@ju.edu.sa

Received 14 January 2021; Revised 9 March 2021; Accepted 22 March 2021; Published 28 May 2021

Academic Editor: Stefano Galassi

The aim of this paper is to assess the structural behavior of hybrid thin-walled beams which were fabricated using laminated carbon fiber reinforced polymer (CFRP). Seven hybrid (CFRP) I-beams were fabricated, instrumented, then have been tested under monotonic four-point loading in order to evaluate their behavior up to failure. In constructing the I-beam specimens which were evaluated in this study, plywood core was implemented on both the web and flanges. Several important parameters were conducted in this study considering changing both of the ply orientations and stacking sequences of laminated fibers, also changing the shear span-to-depth ratio (a/d) of the specimens. The experimental results showed that stacking sequence is the most significant parameter that influences both flexural strength and stiffness of the hybrid beams. Also, the experimental results promoted the effectiveness of the core material for enhancing the flexure (bending) stiffness of beams. Then, these results were compared with a previous simulated study which used the finite element modeling to model the beams. Also, in order to evaluate the efficiency of the CRFP beams, the results were compared to similar steel beams having the same dimensions of the CFRP beams. As compared to steel beams, the load carrying capacity of the laminated beams is being high compared with steel beams when taking into consideration their specific strength ratio.

1. Introduction

In the last few years, there has been widespread use of FRPs in the construction field for different structural proposes, including the repair of existing damaged concrete members, as well as the erection of new structures entirely made of FRP. FRP composites have many advantages, such as electromagnetic transparency, highly resistance to corrosion, low costs of maintenance, and high strength-to-weight ratio for composite members which is the main advantage.

Several research studies have been studied and focused on the performance of FRP thin-walled beams, and many relevant research studies have been conducted on optimizing the behavior of the composite sections. For example, Hai et al. [1] have performed bending tests on a group of hybrid carbon-glass FRP I-beams including variable carbon fiber contents in their flanges. The increase in the amount of carbon fiber (CF) had a direct effect for higher bending stiffness of the beams; the maximum load capacity was conducted for 33% content of CF.

Nuno et al. [2] have studied the performance of hybrid fiber-reinforced polymer five series I-beams under flexure. These I-beams had different types and sequences of GFRP I-section profiles with mats reinforcing. The series beams have made from both glass fiber and carbon fibers and then pultruded together by embedding them in a polyester matrix. All series of beams showed higher bending stiffness than all GFRP I-section profiles (reference beams).

Combined numerical and experimental studies about the behavior of glass FRP beam and hybrid carbon-glass FRP

beam with unidirectional (CF) mats have been carried out by Correia [3] and Nunes [4]. Numerical finite element models showed good acceptable results with the experimental study for terms of stiffness and ultimate load. When studying the effect of orientation and direction of fibers, Aktas [5] has found that because of decreasing beam stiffness, the deflection of the beam has been increased for fiber orientation angles from 0° to 90°.

Recently, several codes dealing with design methods and equations and safety factors for hybrid fiber-reinforced polymer composite elements have been developed. In 1996, the Euro Comp Design Code and Handbook [6] was published, and it included many guidelines for the structural design of polymer compounds. After that, in 2002, the CEN 13706 standard [7] did not provide any design guidelines. However, the CEN 13706 standard stated two different classification of materials, according to the minimum values for properties of materials. Then, the Italian National Research Council (CNR) was published in 2007, and its Design Manual (DT 205/2007) deals with the design of pultruded FRP structures [8]. In 2010, the ASCE published (MOP) #102 which focused on Manuals of Practice for the designing of FRP composite connections [9].

This paper studied the response of hybrid (CFRP) laminated thin-walled I-beams. Seven different (CFRP) beams were studied experimentally and analytically and compared the results with a previous simulated study conducted by Yosri, A.M et al. [10] which used the finite element modeling to model the beams. Also, in order to evaluate the efficiency of the CRFP beams, the results were compared to similar steel beams having the same dimensions of the CFRP beams.

2. Experimental Program

2.1. Experimental Parameters and Details of Beam Specimens. A series of seven (CFRP) laminated composite I-beams with 1,200 mm supported length have been studied in this research. The I-section had dimensions of 200 mm (web height), 100 mm (flange width), 5 mm (wall thickness), and 10 mm (flange thickness). The core material of these I-beams was from plywood which has been used in both of web and flanges. The reinforcement material in this experimental program was from laminated carbon fiber (CF). This fiber reinforcement was unidirectional woven fibers fabricated with midrange strengths, as shown in Figure 1. The resin used in fabricating the specimens had two components: (i) thixotropic epoxy-based impregnating resin and (ii) a catalyst. The polyester comes in tins each weighting 5.0 kg.

Table 1 lists detailed information about the specimens. As shown in this table, in order to study the efficiency of the composite beams, the bending test was carried out on two steel I-beams (S1 and S2) with the same dimensions to make a comparative study in terms of specific strength ratio.

2.2. Specimen Assembly

2.2.1. Preparation of Matrix. The resin of composites has two components. The primary is the matrix (A), and the second is the hardener (B). Mix components A + B together for at the least three minutes until the material becomes smooth in consistency and a uniform gray coloration as shown in Figure 2.

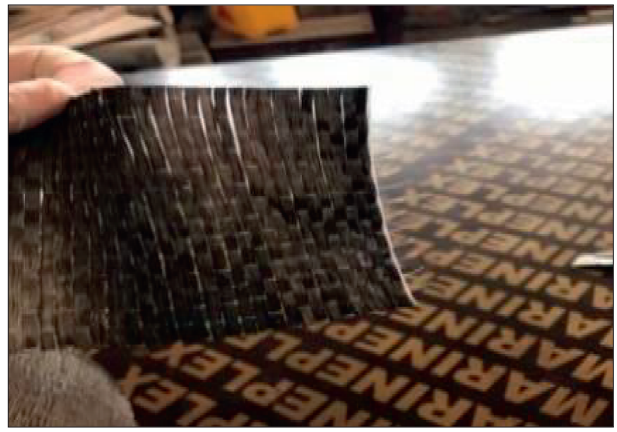

Figure 1: Unidirectional woven carbon fabrics.

2.3. Preparation of Specimens. As shown in Figure 3, the core section was manufactured with specific dimensions. The resin was coated on the wood, and then first ply was cut to cover all sections at the same time after applying resin (so that the direction of the fiber is parallel to the beam axis 0°). After this, again the coating of resin was done. The laminates had been fabricated by putting the plies one over the other with a matrix in between the layers, and the process is continued until the specified thickness was obtained. All of the web laminate plies have been extended through the web/flange interface, becoming a part of flange laminates.

2.4. Material Properties. The CFRP laminates were from unidirectional fiber (carbon/epoxy) with a thickness of 0.129 mm. The mechanical properties of the laminates have been listed in Table 2. For bonding all the laminates, they were implemented with epoxy adhesives in room-temperature cure.

2.5. Tests Setup and Procedure. All of beams were tested under a four-point bending on a test set up of simply supported steel rigid frame as shown in Figure 4. Two sets of plates and rollers were used for supporting each beam. A wide flange spread beam which is placed on two steel plates and covering the entire width of the beam has been used to make two-point load setup. The load was generated by a hydraulic jack (capacity of 500 kN). The applied load has been measured using a load cell attached to this hydraulic jack. Steel beam (IPE) was used for transferring the applied load to the beams.

In order to measure the deflections under the loaded sections, three linear variable differential transformers (LVDT) were used. Then, four electrical strain gauges were installed and bonded at different positions to measure both of bending behavior and shear behavior of the beams and to

Table 1: Detailed information about the specimens.

Group	Shear pan to depth ratio (a/d)	Beam	Lay-up of the flanges	Lay-up of the web
A	2	S1	Steel beam	
		S-A-1	$(0, 90, 0_2, 90)$	$(0, 90, -45, 45)_s$
		S-A-2	$(0, 90, 0_3, 90)$	$(0, 90, -45, 45)_s$
		S-A-3	$(0, 90, 0_4, 90)$	$(0, 90, -45, 45)_s$
B	1	S2	Steel beam	
		S-B-1	$(0, 90, 0_2, 90)$	$(0, 90, -45, 45)_s$
		S-B-2	$(0, 90, 0_2, 90)$	$(0, 90, \pm45, \pm45)_s$
		S-B-3	$(0, 90, 0_2, 90)$	$(0, 90, \pm60)_s$
		S-B-4	$(0, 90, 0_2, 90)$	$(0, 90, \pm60, \pm60)_s$

Figure 2: Preparation of the matrix.

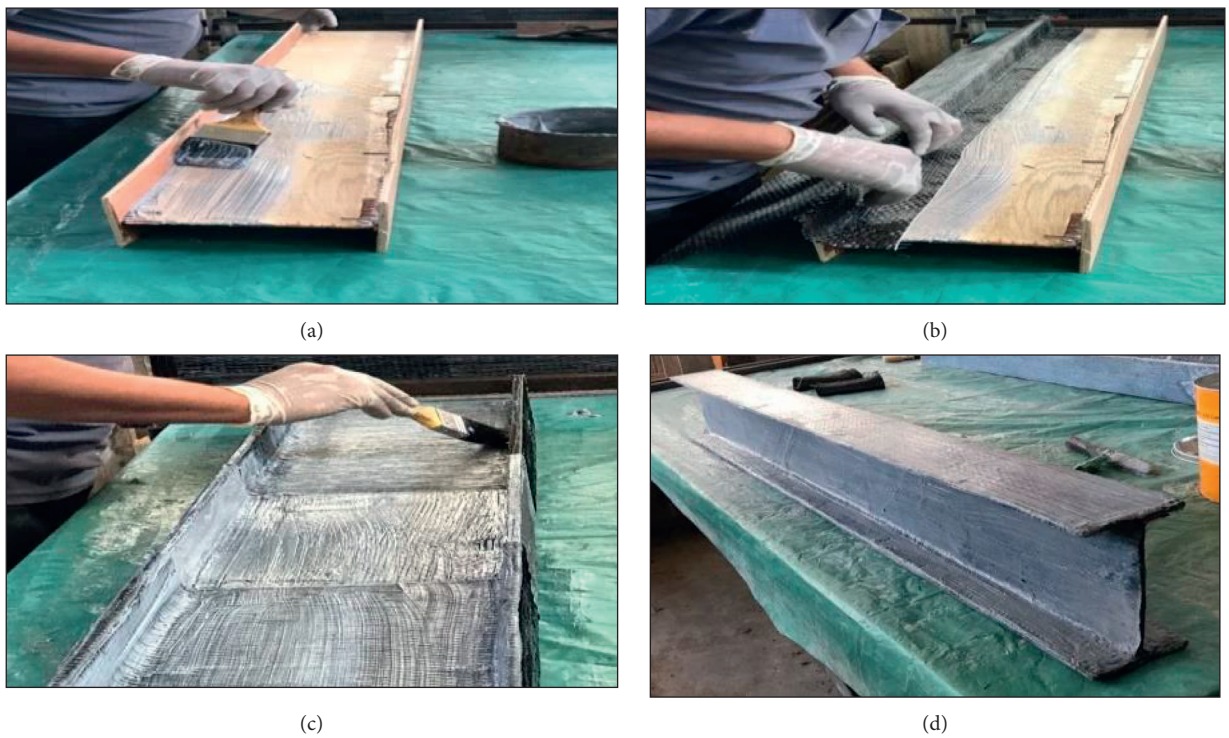

(a) (b) (c) (d)

Figure 3: Preparation of specimens. (a) The resin was coated on the wood. (b) Fiber sheet (first ply) was placed on the coating. (c) Putting the plies one over the other with a matrix. (d) Hybrid CFRP laminated I-beam.

Table 2: Properties of the laminate.

Property		Direction	
		1-1	2-2
Tensile	Failure stress (MPa)	2231	29
	Longitudinal modulus of elasticity (MPa)	130800	15000
Compressive	Failure stress (MPa)	1082	100
	Failure strain (%)	1.08	1.92

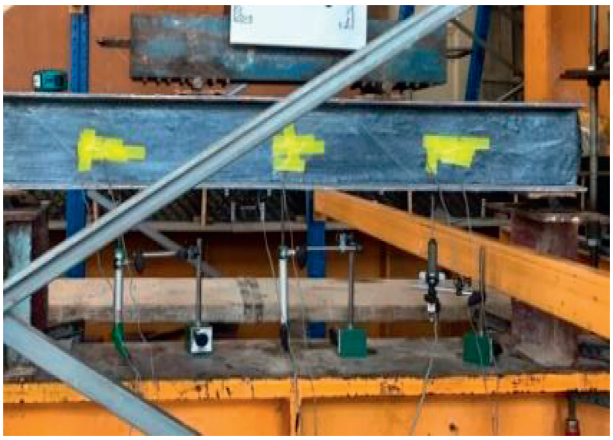

(a)

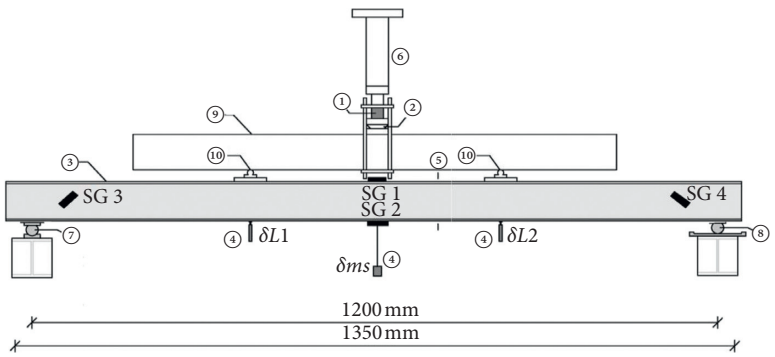

① Load cell
② Spherical hinge
③ Specimen
④ Displacement transducers (| or |)
⑤ Section equipped with strain gauges
⑥ Hydraulic jack
⑦ Fixed support
⑧ Rolled support
⑨ Load distribution steel beam
⑩ Load application plates and hinges

(b)

Figure 4: (a) Setup of testing and (b) details and locations of strain gauges.

monitor the damage initiation and also the damage propagation. Finally, we use a calibrated data acquisition system for collecting all data and use a data logger system for collecting all the instrumented data.

3. Experimental Results

3.1. Modes of Failure and Cracks Pattern. Modes of failure and growth of cracks were reported for the group A beams

and group B beams. For group A beams with (a/d) ratio equal two, it was observed that the delamination cracks were developed at the core material. Cracks in the wood were occurred when tensile strains exceeded the wood capacity. This cracks induced radial stresses in the web-bottom flange junction causing delamination of the laminates, due to the incapability of laminates to absorb the released energy, leading to separation between them. The beam failed without increasing further loads. Furthermore, the failure occurred at the junction of web-bottom flange as shown in Figure 5(a).

For group B beams, the observed failure modes can be stated as delamination failure and local compression buckling failure. In the case of both the S-B-1 and S-B-2, the compressive stresses caused localized web buckling. This type of buckling behavior leads to reduce effective stiffness of the web and, therefore, hurried the failure of beams. Due to the influence of the rigidity at the connection junction of web-flange on the magnitude of the buckling loads, the latest failure occurs in material delamination, which is caused due to the effect of the local buckling of the thin wall.

For specimens S-B-2 and S-B-4, the mode of failure observed was transverse shear failure which is caused by the concentrated bearing load conditions and caused local buckling on the compression flange as shown in Figures 5(a) and 5(b). Moreover, it was showed that when the top flange has been buckled, it leads to decrease its stiffness and leads to the neutral axis of the beam to shift to the tension flange. The result of this movement caused accelerating failure of the beam due to an increasing in compressive strain in the buckled flange. Shear cracks were not observed even for group B beams, and the possible reason for this is due to the presence of the inclined plies of ±45 and ±60 orientation which provides a stronger shear resistance along the transverse direction. Table 3 presents a summary of the test results with respect to failure moments, failure loads, and failure modes for all beams.

3.2. Load Deflection. Experimental loads vs. mid-span deflections for different specimens are presented in Figures 6 and 7 , which showed a linear behavior until failure for all beams. The carrying capacity of tested beams was affected by the changing of the shear span to depth (a/d) ratio. All beams show a brittle failure in both flexural and transverse shear failure modes.

The load-deflection curves of S-A-1, S-A-2, and S-A-3 are shown in Figure 6. These beams were fabricated with different stacking sequence in flanges. As shown in this figure, as the flange laminates with 0-degree increased, lower deflection was observed. For example, maximum deflection for S-A-3 was relatively lower than the maximum deflection of beam specimen S-A-1 by 25%. Also, Figure 7 shows the load-deflection curves of group B specimens which were fabricated with different both stacking sequence and ply orientation in webs. One could see that there was a nonlinear response before the final failure for the beams. This behavior is possibly due to the crushing of the specimen at the support and at the loading points which leads to separation of the web-compression flange junction. This progressive failure results in the web to continue carrying the applied load. Due to the effect of number of web plies, the maximum deflection for (S-B-1) was relatively higher than the S-B-2 by 23.2%. However, the deflections of specimens S-B-2 and S-B-4 were the same value. The mainly reason is that the orientation angles of web laminates (45 or 60) did not affect greatly the beam deflection.

3.3. Moment-Strain Behavior. The strain measurements for the beams at the top and bottom flanges in addition to the strain at the shear path are shown in Figures 8–10 . Figure 8 shows the moment-strain curves of S-A-1, S-A-2, and S-A-3 beam specimens. As shown in this figure, all beams showed similar strain behavior. Initially, the behavior showed linear elastic up to the first tensile failure of the wood material was encountered. Due to changing of the tensile modulus of the core material, it caused nonlinearity in the observed tensile strains. This also leads to reduce the stiffness of the hybrid beams. The results showed that, as the bottom flange laminates with 0-degree increased, lower tensile strain was achieved. For example, tensile strain for S-A-3 specimen was lower than tensile strain for S-A-1 specimen by 9% which is because of the effect of increasing the plies number with 0-degree.

Also, the results indicated that decreasing shear span led to the decrease in tensile strain. The shear strain increased with low shear spam to depth ratio due to deformation of an inclined strut that transfers a large portion of the shear is transferred directly to the support. The results showed that the compressive strain for beam specimen (S-B-2) was relatively lower than the deflection of S-B-1 by 25% as shown in Figure 9, and the compressive strain for beam specimen S-B-4 was relatively lower than the deflection of S-B-3 by 20%, meaning that increase of the number of web laminates with 45-degree is more effective than increase of the number of web laminates with 60-degree. Figure 10 presents the normalized strains from the rosettes on specimens of group B. As shown in this figure, as the web laminates' orientation angle decreased, higher rosette strain was achieved. For example, due to the effect of number of web plies with 45°, the rosette strain for S-B-3 was fewer than rosette strain from S-B-1 by 10.2%.

4. Analytical Modeling and Finite Element Analysis (FEA)

4.1. Prediction of Beam Stiffness. The beam stiffness is determined by Young's modulus (E) and moment of inertia (I). According to Jitesh [11], the beam stiffness is expressed as D_x^c. The beam stiffness can be determined using the Classical Lamination Theory (CLT) as follows:

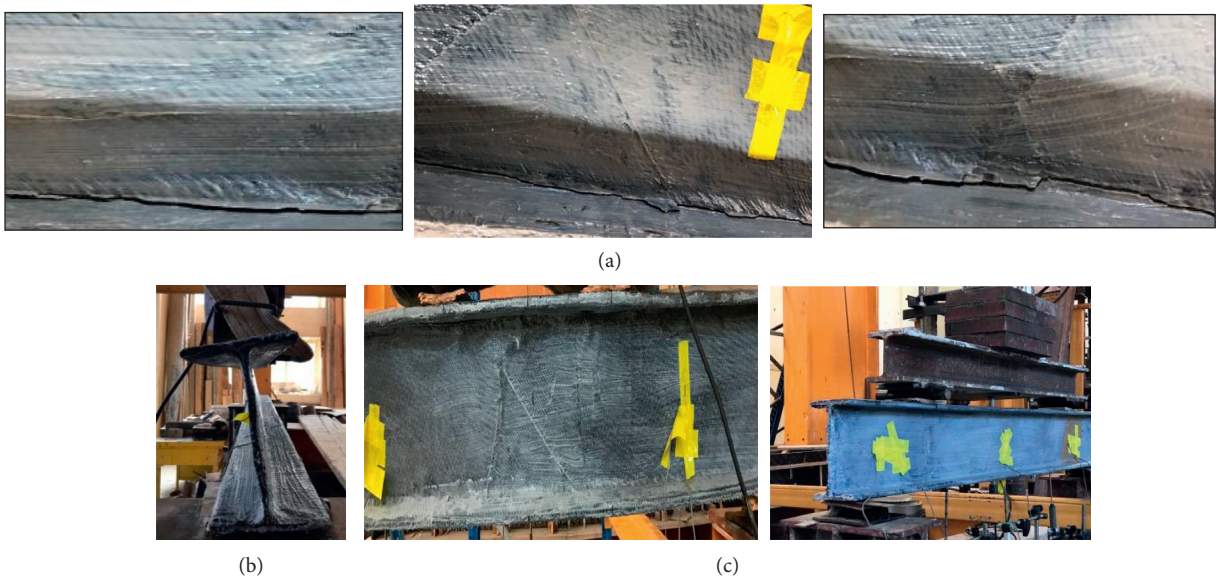

(a)

(b) (c)

Figure 5: (a) Delamination cracks in group A beams. (b) Localized buckling of the web for S-B-1 and S-B-3 and (c) failure in group B beams. Local buckling on the compression flange for S-B-2 and S-B-4.

Table 3: Failure moment and load results for tested beams.

Case no.	Specimen	Failure[1] load (KN)	Failure moment (kN·m)	Failure mode
Group A	S-A-1	17.3	3.46	Delamination[2]
	S-A-2	20.8	4.16	Delamination[2]
	S-A-3	25	5	Delamination[2]
Group B	S-B-1	24.6	2.46	Delamination[3]
	S-B-2	26.64	2.66	Compression[4] buckling
	S-B-3	28	2.8	Delamination[3]
	S-B-4	29	2.9	Compression[4] buckling

[1]The total failure loads on the beam (cell load) which is equal to 2P. [2]Delamination at the web-bottom flange junction. [3]Delamination at the web-top flange junction led to the localized buckling of the web. [4]The beam failed with a huge compression buckling of top flange.

$$D_x^c = \left\{ b_{f1}\left(A_{1,f1}^* z_{1c}^2 + 2B_{1,f1}^* z_{1c} + D_{1,f1}^*\right) + b_{f2}\left(A_{1,f2}^* z_{2c}^2 + 2B_{1,f2}^* z_{2c} + D_{1,f2}^*\right) + A_{1,w}^*\left(\frac{h_w^3}{12} + h_w h_{wc}^2\right)\right\}, \quad (1)$$

where b_f = flange width and h_w = web height. Note that A_1^*, B_1^*, and D_1^* refer to the axial, coupling, and bending stiffness's for each sublaminates of the beam and were determined based on CLT, where z_{1c}, z_{2c}, and h_{wc} are the distances from midplane of each of top flange, bottom flange, and web, respectively, to centroid of the cross-section as shown in Figure 11.

4.2. Prediction of Deflections. As the composite materials with unidirectional direction have a few ratio of shear modulus to longitudinal modulus that leads the beam deflection due to shear to be increase when increasing in its anisotropic ratio. Mottram [12] confirmed that there will be a potential risk in the analysis of FRP beams if the shear deformation is not considered.

In this study, the deflection of the beams was computed based on Timoshenko's beam theory, which takes shear deformation into consideration. The Timoshenko equation [13] showed that, for a four-point bending test, the loads applied at the third points can be presented as follows:

$$\hat{o}_{max} = \hat{o}_{flexure} + \hat{o}_{shear} = \frac{23PL^3}{1296D_x^c} + \frac{PL}{6kGA}, \quad (2)$$

where D_x^c = stiffness of the beam, G = shear modulus, k = shear correction factor, kGA = shear stiffness, and A = shear area (web cross-sectional area).

4.3. Finite Element (FE) Modeling and Comparisons. In this part of the study, the experimental results will be compared with the results of the finite element study that was conducted by Yosri et al. [10]. In their study, the hybrid laminated CFRP beams were modeled using ANSYS. Both of web and flange used 8-node composite brick elements with different CFRP plies. The finite element geometry and mesh

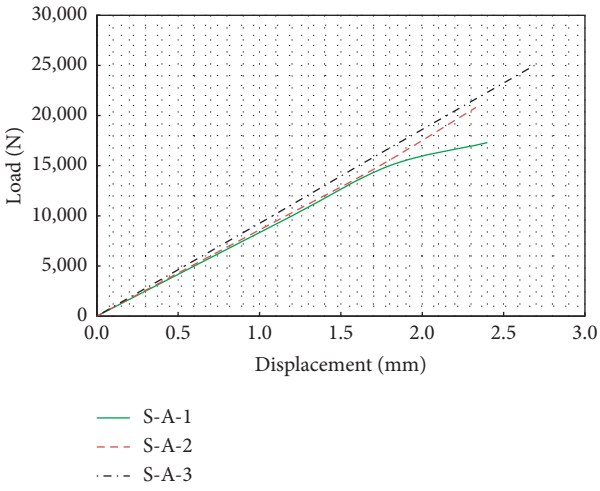

Figure 6: Load-deflection of group A beams.

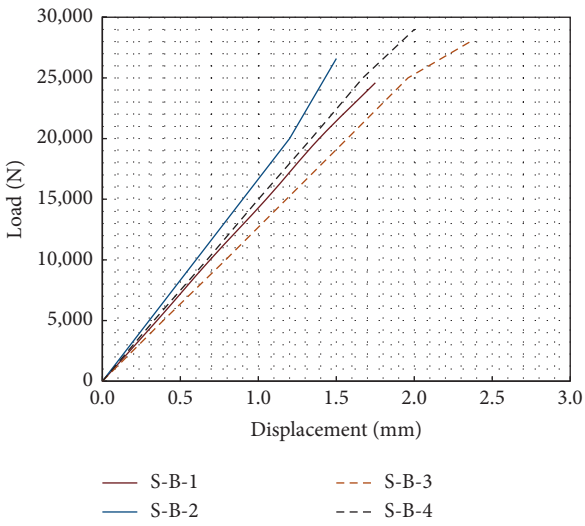

Figure 7: Load-deflection of group B beams.

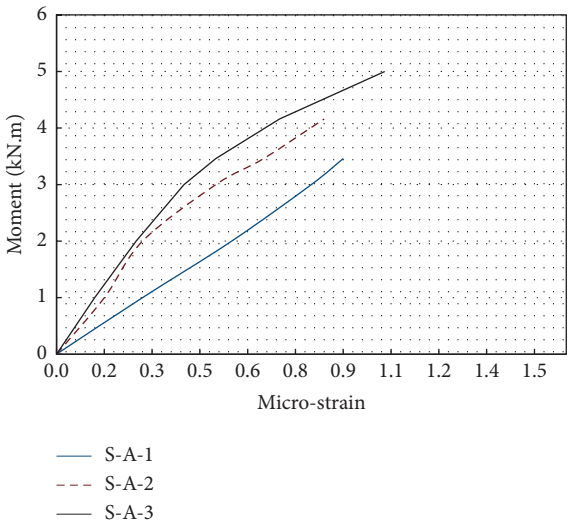

Figure 8: Relation between moment and strain at midspan of the bottom flange (group A beams).

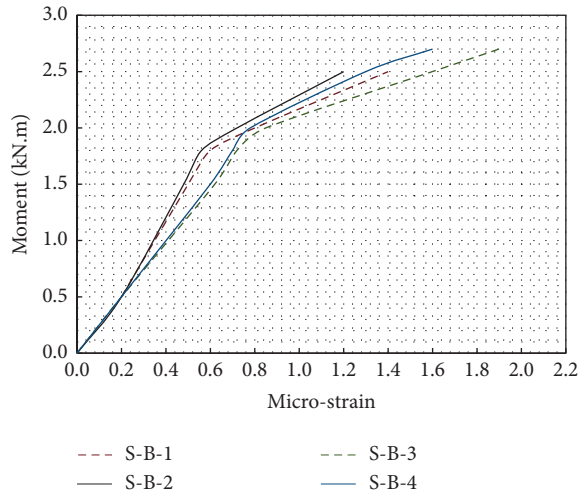

Figure 9: Relation between moment and strain at midspan of top flange (group B beams).

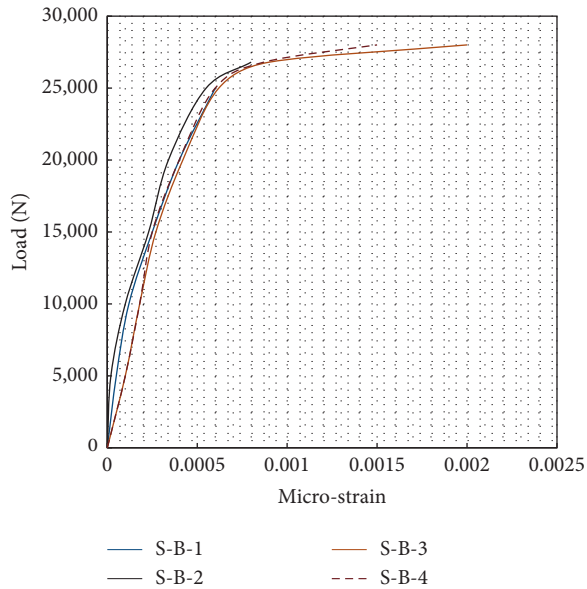

Figure 10: Load-rosettes strain for group B.

with the local coordinate systems 11, 22, and 33 were modeled as shown in Figure 12. The beam meshes were with 10 : 10 (mm) as length-to-width ratio. Finally, the beams were presented from 7368 elements and 11901 nodes. Table 4 shows the properties considered for laminated material and core material, where ν_{ij} is the Poisson ratio, E_i is Young's modulus, $X_{t,i}$ and $X_{c,i}$ are the tensile and compressive strengths, respectively, G_{ij} is the shear modulus, and S_{ij} is the shear strength. The study has obtained these properties from the mechanical characterization tests.

Both of load-deflection curve and bending stiffness which were obtained from the experiment, FE analysis, and theoretical calculations were compared for all specimens. The results are presented in Figures 13 and 14 . From these figures, one can see that both of deflection and bending

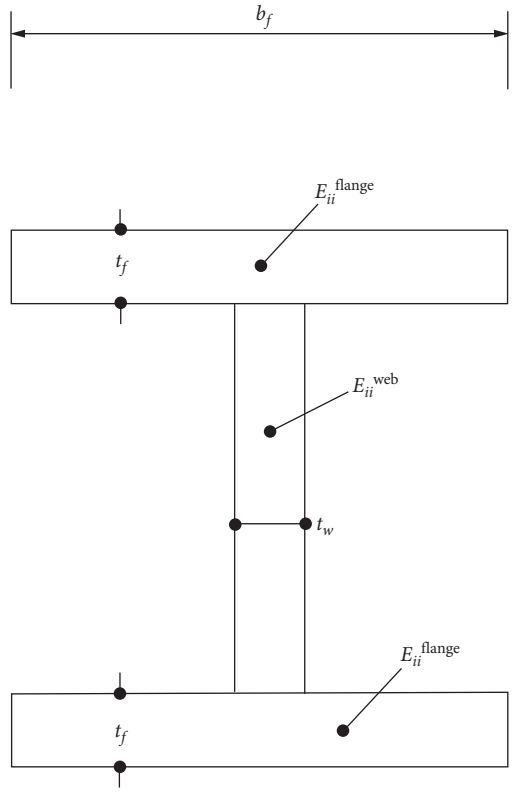

Figure 11: Typical details of beam specimens.

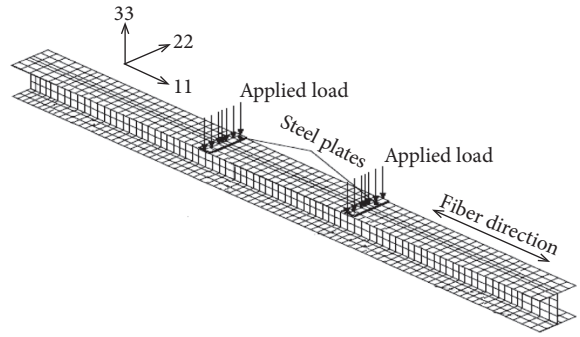

Figure 12: Finite element geometry and mesh (Yosri et al. [10]).

Table 4: FE analysis (input data) (Yosri et al. [10]).

	Units	Notation	Value
Young's modulus	MPa	E_{12}	130780
		$E_{22} = E_{33}$	15000
Poisson's ratio		ν_{12}	0.27
		$\nu_{23} = \nu_{31}$	0.05
Shear modulus	MPa	$G_{12} = G_{23} = G_{31}$	5590
Max. tensile stress (X)	MPa	X_t	2231
Max. tensile stress (Y, Z)	MPa	$Y_t = Z_t$	29
Max. compressive stress (X)	MPa	X_c	1082
Max. compressive stress (Y, Z)	MPa	$Y_c = Z_c$	100
Max. shear stress (XY, YZ, ZX)	MPa	$S_{12} = S_{23} = S_{13}$	60

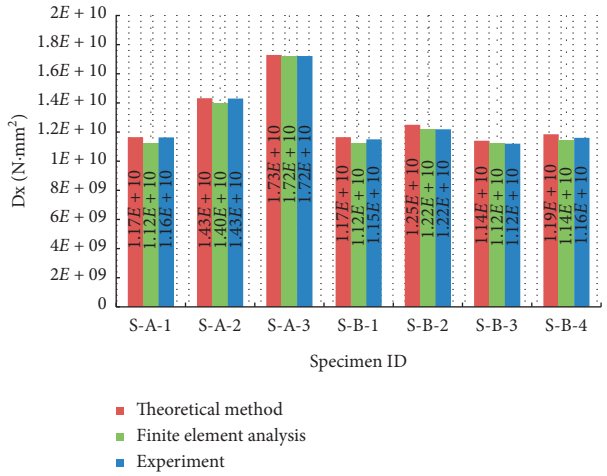

Figure 13: Experimental vs. simulated-theoretical results for bending stiffness.

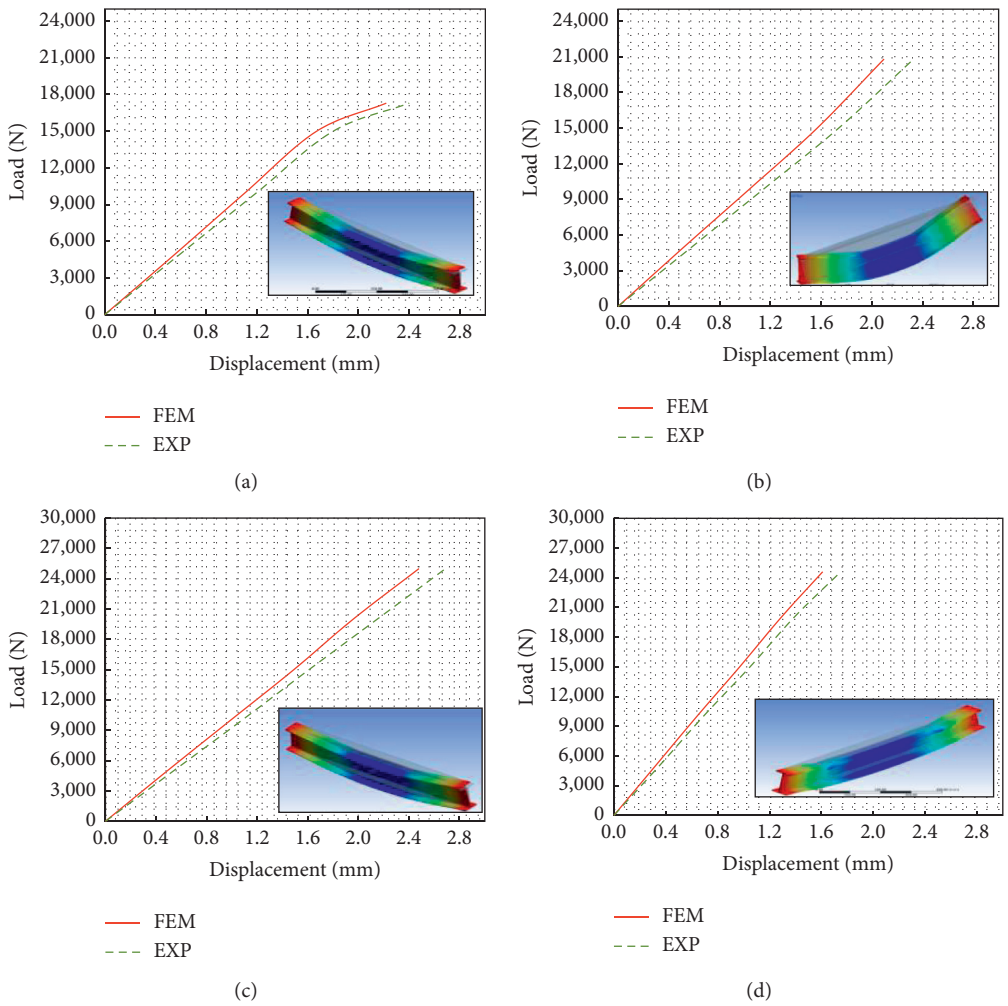

Figure 14: Continued.

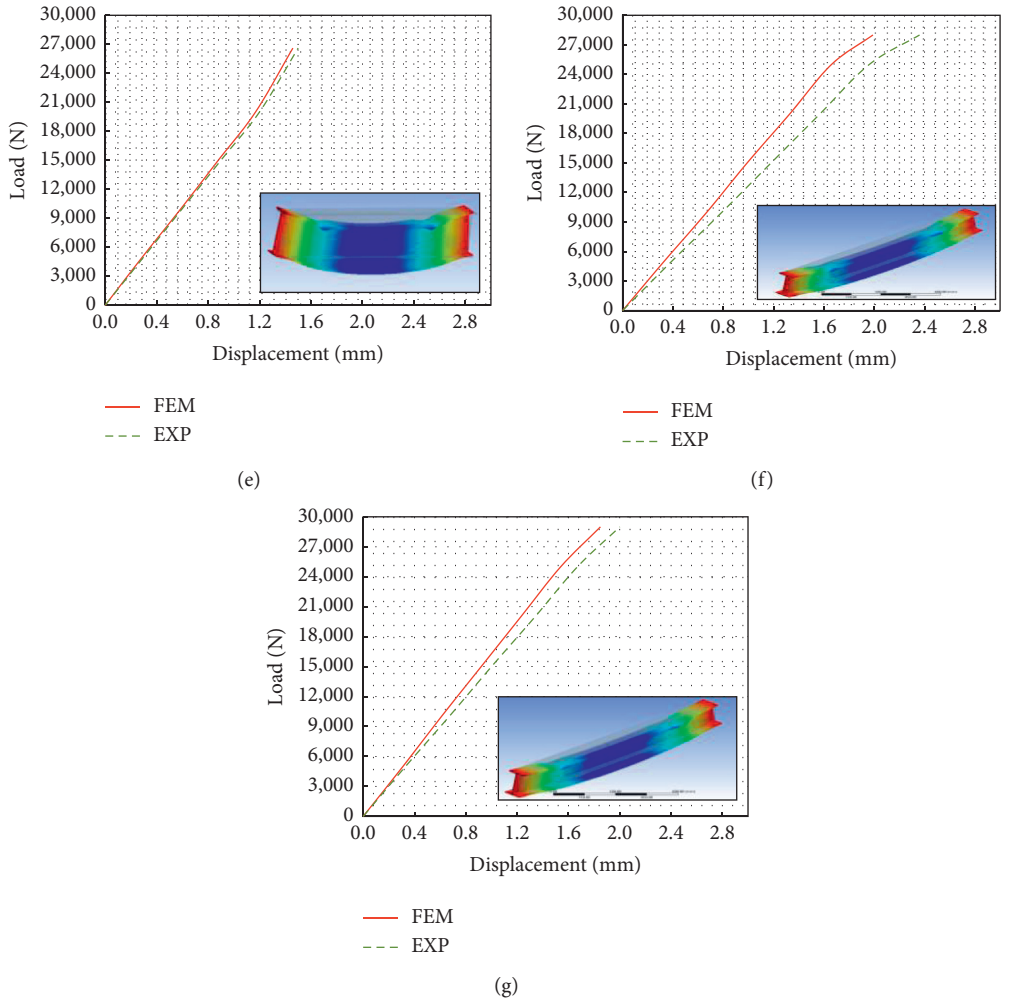

Figure 14: Load-deflection for all specimens. (a) Load-deflection (S-A-1). (b) Load-deflection (S-A-2). (c) Load-deflection (S-A-3). (d) Load-deflection (S-B-1). (e) Load-deflection (S-B-2). (f) Load-deflection (S-B-3). (g) Load-deflection (S-B-4).

Table 5: Specific strength ratio results for tested beams.

Case no.	Specimen ID	Specimen weight (kg)	Specific-strength ratio
Case one	S1 (control)	36	3.38
Case two/group A	S-A-1	4.6	3.76
	S-A-2	5.1	4.07
	S-A-3	5.7	4.38
Case three	S2 (control)	36	3.83
Case four/group B	S-B-1	4.8	5.125
	S-B-2	5.8	4.59
	S-B-3	6.3	4.44
	S-B-4	6.7	4.32

stiffness results observed from the experimental gave less stiff behavior than the finite element results. This can be attributed to several factors including the semirigid behavior of the junction of flange/web that was not included in the FE model. In typical commercial FE codes such as ANSYS, the web/flange junctions are assumed to be rigid with no relative rotation that results in producing results with relatively higher stiffness (MOP 102).

5. Comparative Study

Laminated composite I-beams are more efficient than steel I-beams because of its higher specific strength and specific stiffness in addition to its relative superiority in corrosion resistance. Specific strength ratio is used as a tool for determining the efficiency of the sections. This ratio means that the amount of load can be sustained per increase in self-

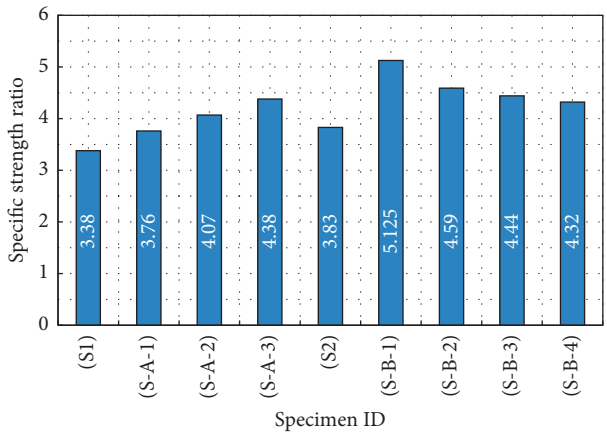

Figure 15: Specific strength ratio for all specimens.

weight of the section, which means that higher the ratio, greater the performance of the section. For evaluating the efficiency of the composite sections as compared to comparable steel sections in terms of strength-to-load ratio, bending tests were performed on two steel I-beams (S1 and S2) with similar dimensions to the same composite beams. Table 5 and Figure 15 show specific strength ratios for all tested beams. The properties of the steel beams are as follows:

Yield strength = 229.0 N/mm^2

Poisson's ratio = 0.3

Cross-sectional area = 2,900.0 mm^2

Modulus of elasticity = 2×10^5 N/mm^2

Modulus of rigidity = 0.769×10^5 N/mm^2

Moment of inertia = 2.63×10^6 N/mm^2

As compared to steel beams, the hybrid laminated beams (HCFRP) are relatively high in load carrying capacity that, incase of considering specific strength of (HCFRP) and its specific stiffness ratio, from Figure 15, and Table 5, it was found to be efficient for using a composite beams due to specific strength ratio, including self-weight, as compared to other steel beams studied. They save about 29% to 51% of the specific strength ratio compared to other steel beams.

6. Conclusions and Recommendations

In this study, different laminated thin-walled I-beams were fabricated, analyzed, and tested in 4-point bending to study its behavior. The experimental behavior of such beams was compared with the simulated study which was conducted by Yosri et al. [10]. The parametric study was included changing the laminates stacking sequence and changing the laminates ply orientations and studied those effects on the behavior of HCFRP beams. Furthermore, we study the effectiveness of changing of shear span to depth ratio on the overall performances of HCFRP beams. Also, in order to evaluate the efficiency of the (HCFRP) laminated beams as compared to a comparable steel beams in terms of strength-to-load ratio, bending tests were performed on two steel I-beams (S1 and S2) with similar dimensions to the same composite beams. The following are concluded in this work:

(i) As compared to steel beams, the carrying capacity of (HCFRP) laminated beams is considered high when taken into consideration the specific strength ratio of (HCFRP).

(ii) At the shear span-depth (a/d), equal (2.0), the deflection has been decreased when increasing the number of flanges plies. The lowest deflection occurred for S-A-3 and specimen S-B-2.

(iii) At the shear span-depth (a/d), equal (1.0), changing the orientation angles of web plies (45° or 60°) does not affect the deflection of beams.

(iv) At the same load, the tensile strain of specimen S-A-1 at the lower bottom flange was bigger than strain of S-A-3 by 8.0% that was due to the effect of increasing the number of plies with 0-degree.

(v) At the span to depth ratio (a/d) equal (1.0), the majority of the beams failed due to local compression buckling of top flanges and delamination of the web laminates. The increase of the number of web laminates with 45° causes the decrease in the compression strain by 25.0%.

(vi) At the shear span-depth (a/d), equal (2.0), the bending stiffness was increased by 59% as the number of flange plies with 0-degree increase.

(vii) Decreasing the angles of web plies leads to increase bending stiffness of beams, the results also showed that when the plies angles of the web are greater than 45°, and the decrease of the bending stiffness will become.

(viii) Decreasing the angles of web plies leads to increase the shear resistance, when the plies angles of the web are greater than 45°, the decrease of the shear resistance will become.

(ix) The use of wood in the I-beam provided adequate stability to the section, and it was appears to be a cost-effective method to increase flange and web thickness in order to eliminate second-order failures.

(x) The results showed that the present experimental method of HCFRP laminated composite beams was viable for fabricating these beams, and according to the previous results and this study applications, the research recommends the following possible items that could be put under consideration as follows.

(a) It is highly recommended to use either a high-density balsa wood core or ultrastrength polymeric mortar.

(b) It is highly recommended to study more specimens with various plies.

(c) It is highly recommended to study more specimens with different span to depth ratios.

(d) It is highly recommended to study more specimens with different types of fibers.

(e) Focus on studying the web/flange local failure.

(f) Study the durability of hybrid laminated FRP thin-walled I-beam.

(g) Study the impact resistance of hybrid laminated FRP thin-walled I-beam.

Data Availability

The data used to support the findings of this study are included within the article and are available from the corresponding authors on reasonable request.

Ethical Approval

This article does not contain any studies with human participants performed by any of the authors.

Conflicts of Interest

All authors declare that they have no conflicts of interest.

Acknowledgments

The authors extend their appreciation to the Deanship of Scientific Research at Jouf University for funding this work through research grant no DSR-2021-02-0119.

References

[1] N. D. Hai, H. Mutsuyoshi, S. Asamoto, and T. Matsui, "Structural behavior of hybrid FRP composite I-beam," *Construction and Building Materials*, vol. 24, no. 6, pp. 956–969, 2010.

[2] N. Silvestre, F. Nunes, S. Asamoto, and R. João, "Correia structural behavior of hybrid FRP pultruded beams: experimental, numerical and analytical studies thin-walled structures," 2016.

[3] M. M. Correia, *Structural Behavior of Pultruded GFRP Profiles: Experimental Study and Numerical Modeling*, Instituto Superior Técnico, London, UK, 2012.

[4] F. F. Nunes, *Comportamento e structural de perfis pultrudidos de GFRP re-forçados com mantas de CFRP Caracteriz ação experimental e modelação numérica*, Instituto Superior Técnico, London, UK, 2012.

[5] A. Aktas, "Determination of the deflection function of a composite cantilever beam using the theory of anisotropic elasticity," *Mathematical & Computational Applications*, vol. 6, no. 1, pp. 67–74, 2001.

[6] Eurocomp Design Code and Handbook, *Structural Design of Polymer Composites*, The European Structural Polymeric Composites Group, London, UK, 1996.

[7] European Committee for Standardization (CEN), EN 13706, *Reinforced Plastics Composites-Specifications for Pultruded Profiles. Part 1: Designation; Part 2: Methods of Test and General Requirements; Part 3: Specific Requirements*, CEN, Brussels, Belgium, 2002.

[8] Technical Document CNR-DT 205/2007, *Guide for the Design and Construction of Structures Made of FRP Pultruded Elements*, Italian National Research Council (CNR), Rome, Italy, 2008.

[9] A. S. Mosallam, *Design Guide for FRP Composite Connections. Manuals of Practice (MOP) 102*, American Society of Civil Engineers (ASCE), Rome, Italy, 2011.

[10] A. M. Yosri, G. M. Ghanem, M. A. E. Salama et al., "Structural performance of laminated composite thin-walled beams under four-point bending," *Innovative Infrastructure Solutions*, vol. 4, p. 58, 2019.

[11] C. P. Jitesh, *Stress Analysis of Laminated Composite Beam with I-Section*, The University of Texas at Arlington, Houston, Texas, UK, 2010.

[12] J. T. Mottram, "Lateral-torsional buckling of a pultruded I-beam," *Composites*, vol. 23, no. 2, pp. 81–92, 1992.

[13] M. D. Hayes and J. J. Lesko, "Measurement of the Timoshenko shear stiffness. I: effect of warping," *Journal of Composites for Construction*, vol. 11, no. 3, pp. 336–342, 2007.